Lafia Journal of Scientific & Industrial Research (LJSIR), Vol. 4(1), 2026
p-ISSN: 3026 – 9288 e-ISSN: 3027 – 1800 pages: 198–205
https://lafiascijournals.org.ng/index.php/ljsir/index ⇒ Published by the Faculty of Science,
Federal University of Lafia, Nasarawa State, Nigeria

First-principles Computation of Cubic $CsGeF_3$ Perovskite's Structural, Elastic, and Mechanical Properties

M. S. Otto[1]*, M. S. Liman[1], Abdullahi Lawal[2], A. D. Abdullahi[1] & F. M. Usman[1]
[1]Department of Physics, Federal University of Lafia, Nasarawa State, Nigeria
[2]Department of Physics, Ahmadu Bello University Zaria, Kaduna State, Nigeria

Abstract

The research investigates the structural, elastic and mechanical characteristics of lead-free cubic $CsGeF_3$ perovskite under density functional theory (DFT) through combined Quantum Espresso and Thermo_PW computational techniques. The researchers conducted three exchange-correlation functional tests (PZ, PBE, and WC) to determine lattice parameter optimization, elastic constant computation and mechanical stability assessment. The research showed that optimized lattice constants achieved results which closely aligned with existing theoretical data. The material's mechanical stability is demonstrated by its predicted elastic constants which require cubic crystal structures to maintain structural integrity. The evaluation of material's mechanical properties used Young's, Shear modulus, and Bulk moduli, Poisson's and Pugh's ratio, machinability index, Vickers hardness test and anisotropy factor measurement. The study found that $CsGeF_3$ can withstand compression while displaying ductile behaviour in certain operational situations. The comprehensive study shows that $CsGeF_3$ functions as a lead-free perovskite which shows potential in optoelectronic devices and solar energy harvesting technologies.

Keywords: Perovskite, Optimization, Elastic constants, First-principles calculation

Article History

Submitted
January 28, 2026

Revised
April 19, 2026

First Published Online
April 22, 2026

Correspondences
M. S. Otto ✉
o.muhammed@science.fulafia.edu.ng

doi.org/10.62050/ljsir2026.v4n1.806

Introduction

Although halide perovskites have emerged as one of the most likely candidates for optoelectronic applications, the investigation of lead-free perovskites has garnered significant attention because of the health and environmental risks connected with lead-based materials [1- 5].

The Inorganic and organic-inorganic halide perovskites have simple crystal structure, strong light absorption and excellent band gap whose, **ABX_3** is general formula of perovskites where, **A** is a larger cation (monovalent), usually an inorganic or organic element Cs^+, NH_4^+, $CH_3NH_3^+$ occupying the corners of the cubic unit cell (Fig. 1). **B** is a smaller cation (bivalent), typically a transition metal like Pb^{2+}, Sn^{2+}, Ge^{2+} sitting at the centre. **X** is an anion, usually a halide ion such as Cl^-, Br^-, F^- or I^- positioned at the faces, forming an octahedral cage around the B ion [1- 5].

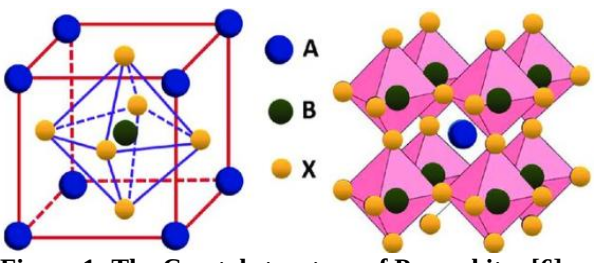

Figure 1: The Crystal structure of Perovskites [6]

Lead-based Perovskites, e.g. $MAPbI_3$ or $CH_3NH_3PbI_3$, $FAPbI_3$ or $CH_3CH_2NH_3PbI_3$, $CsPbI_3$, and others, are the most effective types of perovskites because they have demonstrated remarkable performance (i.e., the highest energy conversion efficiencies) in photovoltaic applications [7-10]. Perovskite solar cells' efficiency has risen from single digits to a certified 22.1 % in just a few years. The study from reference [11] shows that perovskite solar cells experience their main issue because their solar cells lose their operational stability after they function for extended time periods. The challenges include creating testing methods that need standardization and developing methods to prevent ionic mobility from affecting performance during testing and creating methods to counteract material degradation.

Researchers began studying organic-inorganic halide perovskites after they became popular in 2012 because these materials possess exceptional optoelectronic properties which make them suitable for use in photovoltaic applications. Lead (Pb)-based halide perovskite solar cells have demonstrated their commercial value through the achievement of 23 % power conversion efficiency. The toxic properties of lead create a major barrier which prevents lead-based technology from achieving widespread market acceptance [12]. The research field focuses on developing better metal replacements which will

replace lead because of its environmental harm. The germanium (Ge)-based perovskites stand out among alternatives because they possess matching semiconductor characteristics which may exceed their current state [13]. Ge-based halide perovskites have reached their current status as a suitable replacement for tin (Sn) and lead-based materials after scientists conducted extended research and development work over several years.

The researchers investigated $CsGeF_3$ as a lead-free perovskite because this material offers environmentally friendly permanent solutions which match or surpass the excellent characteristics of lead-based materials. The research on cubic perovskite $CsGeF_3$ remains scarce. The research work of [14] represents the major achievement of pioneering computational studies which emerged during that historical period. The researchers performed a complete evaluation of the cubic halide perovskite series $AGeX_3$ which they studied using density functional theory (DFT) with both modified Becke-Johnson (mBJ-GGA) and GGA-PBE methods for their calculations (A = K, Rb, Cs and X = F, Cl, Br). The materials function as direct band gap semiconductors at the R-point because their band gap measurements ranged between 0.79 eV and 2.87 eV. The compounds showed mechanical stability through their ductile properties which exhibited anisotropic behaviour. The optical features of these materials demonstrated their ability to serve as effective materials for optoelectronic devices that work in both visible and ultraviolet light.

Selmani *et al.* (2022) conducted first-principles calculations on Cs-based fluoro-perovskites (M = Ge, Sn, and Pb). The researchers conducted their investigation by using density functional theory (DFT) through ABINIT code with GGA-PBE exchange-correlation functional. The analysis of electronic band structures proved all three compounds to be direct band gap semiconductors which showed their band gap at the R-point in the Brillouin zone. The derived optical properties indicate strong potential for harvesting visible light, identifying $CsSnF_3$ and $CsGeF_3$ as promising absorber materials for solar cell applications. $CsPbF_3$ was discovered to function as an effective UV absorber for UV-selective optoelectronic devices. The study showed that $CsGeF_3$, $CsSnF_3$ and $CsPbF_3$ reached room-temperature ZT values of 0.56, 0.57 and 0.64 respectively. The findings demonstrate their capability to function as energy conversion systems according to [13].

The objective of this study is to theoretically examine the mechanical, elastic, and structural characteristics of cubic $CsGeF_3$ perovskite inside the DFT framework using Quantum Espresso and Thermo_pw. In particular, we calculated a Kohn Sham gap in the context of known GGA_WC, GGA_PBE, and LDA_PZ.

Materials and Methods

Computational Details

A DFT-based computational research was conducted on the cubic perovskite $CsGeF_3$. The Quantum ESPRESSO package, in conjunction with the Thermo_PW module, was used to run convergence tests, optimize geometry, and calculate future property values. Three different exchange-correlation functionals as implemented in Quantum ESPRESSO were used in the investigation: the generalized gradient approximation by the Wu-Cohen (GGA_WC), and Perdew-Burke-Ernzerhof (GGA_PBE), and the local density approximation by Perdew-Zunger (LDA_PZ). Electron–ion interactions were described using ultrasoft pseudopotentials from the PSLibrary within Quantum ESPRESSO, ensuring accurate and efficient treatment of core–valence interactions, with valence configurations of Cs ($5s^2\ 5p^6\ 6s^1$), Ge ($3d^{10}\ 4s^2\ 4p^2$), and F ($2s^2\ 2p^5$). This methodological approach enabled the systematic computation of key material characteristics, including the equilibrium lattice constant (a), tolerance factor, formation energy, the full set of elastic constants (C_{ij}), and the derived elastic and mechanical moduli.

Self-consistent field calculations with various cut-off energy and k-point grid values are used to conduct a convergence test. The Monkhorst Pack Mesh scheme simplifies Brillouin zone sampling through the kinetic energy cut-offs set to 110 Ry (PZ), 160 Ry (PBE), and 120 Ry (WC), with corresponding charge density cut-offs of 880 Ry (PZ), 1280 Ry (PBE), and 960 Ry (WC) obtained from convergence tests and three k-point grid systems 12×12×12 (PZ), 11×11×11 (PBE), and 13×13×13 (WC) which researchers used to achieve the most accurate results while maintaining the structural integrity of their models [15]. To find the optimal atomic positions and lattice constants, structural and lattice optimizations are carried out employing the various exchange correlations previously described. By examining the generated stress, which is analysed to identify the elastic constants, Cij, the elastic behaviour of the perovskite is assessed. Using the Voigt-Reuss-Hill averaging scheme, further elastic and mechanical properties are calculated from these elastic constants.

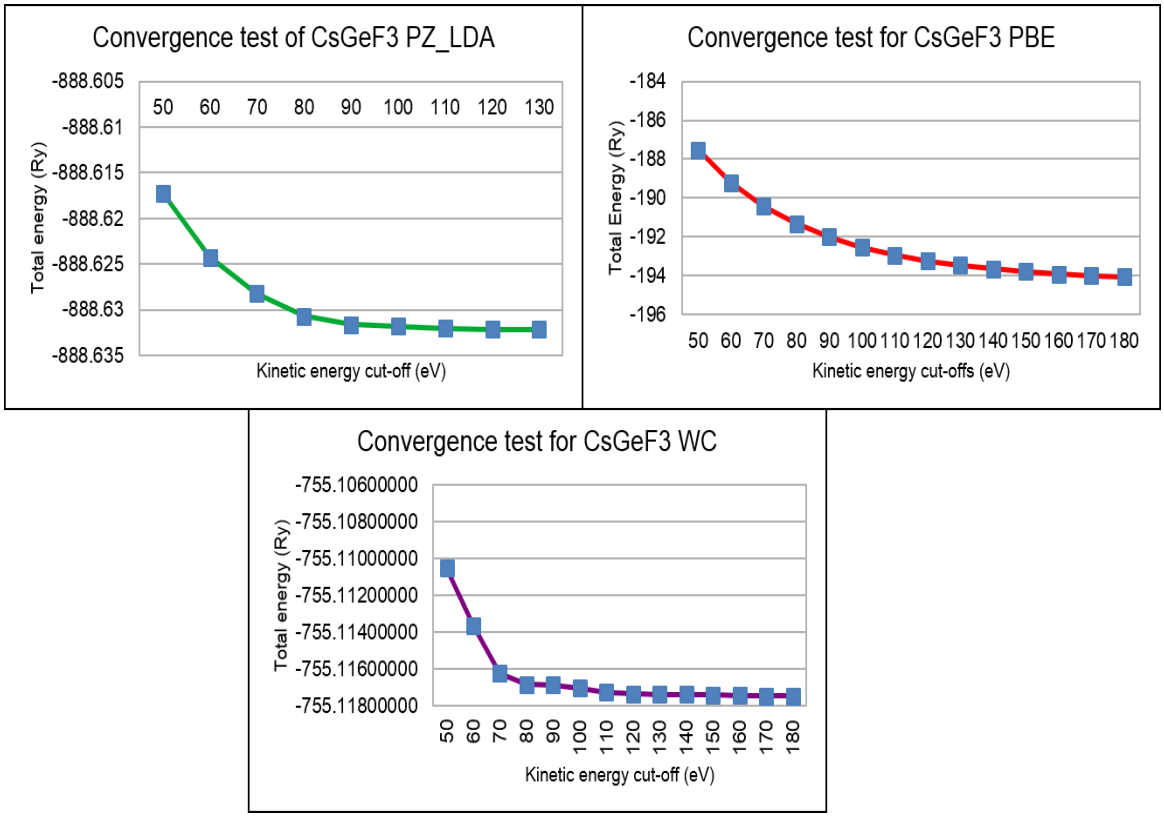

Figure 2: Convergence test (total energy vs kinetic energy cut-off) curve of cubic $CsGeF_3$ with (a) PZ, (b) PBE and (c) WC

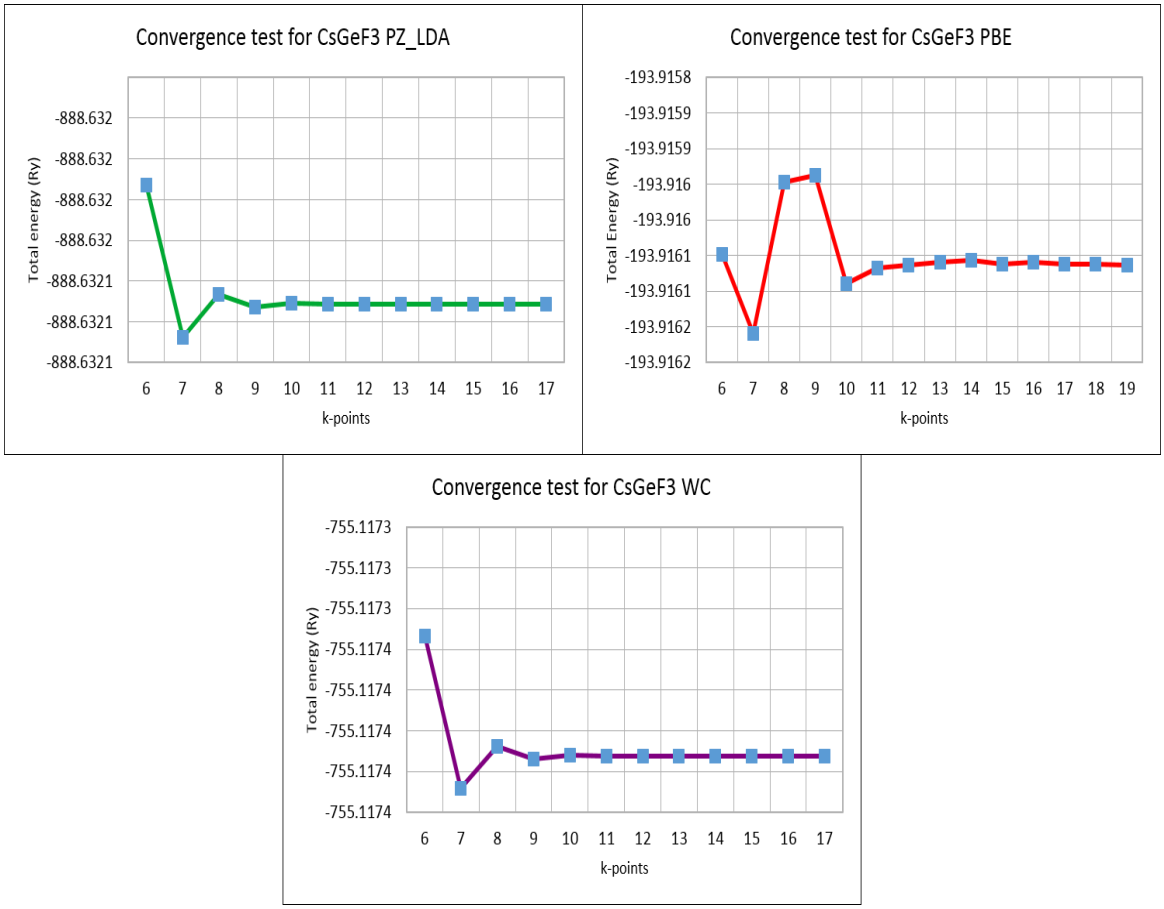

Figure 3: Convergence test (total energy vs k-points) curve of cubic $CsGeF_3$ with (a) PZ, (b) PBE and (c) WC

Results and Discussion

Structural properties

The atomic Wyckoff locations of the cubic $CsGeF_3$ Perovskite unit cell are as follows: Fig. 1 shows the Cs-atom at (0, 0, 0) coordinates with 1a Wyckoff sites, the Ge-atom in the body centre at (0.5, 0.5, 0.5) coordinates with 1b Wyckoff sites, and three F-atoms in the face centre at (0.5, 0.5, 0) coordinates with 3c Wyckoff sites. A geometry optimization process was used to get the equilibrium lattice parameter. The system's total energy (E_{tot}) was calculated as a function of the unit cell volume and the lattice constant (a). The equilibrium value of lattice constant (*a*) corresponds to the minimum on the E_{tot} vs. *a* curve, representing the most stable structural configuration for the given computational parameters.

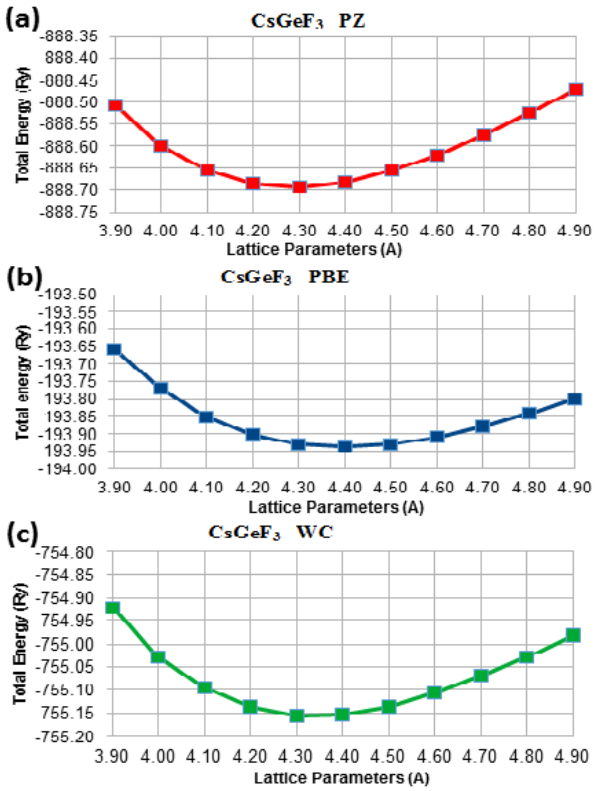

Figure 4: Optimization curve of cubic $CsGeF_3$ with (a) PZ, (b) PBE and (c) WC

Table 1: Optimized structural properties of cubic $CsGeF_3$ calculated using PZ, PBE and WC

$CsGeF_3$ Perovskite	XC functional	a (Å)	Theoretical	Experimental
Present work	PZ-LDA	4.29	—	—
	PBE-GGA	4.33	4.56 [14], 4.57 [13]	—
	WC-GGA	4.34	—	—

The computed total energy for cubic $CsGeF_3$ is shown in Fig. 4 as a function of unit cell volume, obtained using (a) LDA_PZ, (b) GGA_PBE, and (c) WC exchange-correlation functionals. The minimal total energies for $CsGeF_3$ are -888.70 Ry, -193.90 Ry and -754.43 Ry found at lattice parameter values of 4.29 Å, 4.33 Å, and 4.34 Å for PZ, PBE, and WC, respectively. This is consistent with prior theoretical investigations (Table 1).

To confirm the structural stability (e.g. Ionic radii, Tolerance factor (t), Formation energy (E_f)) of the studied perovskite ($CsGeF_3$), we have calculated using the following:

The ionic radii of Cs^+ and Ge^{2+} are calculated by using the formula:

$$R_{Cs^+} = d_{Cs-F} - R_{F^-} \quad (1)$$

$$R_{Ge^{2+}} = d_{Ge-F} - R_{F^-} \quad (2)$$

The ionic radius of Cs^+ is 1.90 Å, calculated from measured bond length, $d_{Cs\text{-}F}$ and the ionic radius of Ge^{2+} is 0.96Å calculated from the measured bond length, $d_{Ge\text{-}F}$ via XCrySDen while the ionic radius of F^- is 1.33 Å obtained by using Shannon radii as a reference.

Tolerance factor (t) [2]:

$$t = \frac{R_{Cs}+R_F}{\sqrt{2}(R_{Ge}+R_F)} \quad (3)$$

Where, R_{Cs}^+, R_{Ge}^{2+} and R_F^- are ionic radii for Cs^+, Ge^{2+} and F^- ions, respectively

The tolerance factors of $CsGeF_3$ for the three (3) different exchange-correlation functionals (PZ, PBE and WC) are listed in Table 2, indicating that $CsGeF_3$ is a structurally stable perovskite because its value falls within the ideal tolerance range of 0.9 – 1.0.

Formation energy, E_f per atom was calculated using the following expression [13]:

$E_f(CsGeF_3) = E_{tot}(CsGeF_3) - [E_{tot}(Cs_{bulk}) + E_{tot}(Ge_{bulk}) + 1.5\ E_{tot}(F_{molecule})]$ 4

E_{tot} $(CsGeF_3)$, E_{tot} (Cs_{bulk}), E_{tot} (Ge_{bulk}), and E_{tot} $(F_{molecule})$ are the computed total energies of $CsGeF_3$ compounds, which contain Cs, Ge, and F. Table 2 shows the predicted formation energy for $CsGeF_3$.

Table 2 deduces the ionic radii, Goldschmidt tolerance factor (t_G) and formation energies (E_{form}) showing the structural and chemical stabilities of $CsGeF_3$ perovskites in PZ, PBE and WC. The values of Goldschmidt tolerance factor are approximately equal to unity (1) within the ideal range (0.9 — 1.0), confirming that the halide perovskite under study is chemically stable. The obtained value of the studied material's formation energy (-3.90 eV/atom) shows a negative sign, which implies that the $CsGeF_3$ perovskite is a more thermodynamically stable material in the cubic phases relative to its elements.

Table 2: Ionic radii, tolerance factor and formation energy of $CsGeF_3$ Perovskite

Perovskites	Ion	Radius (Å)	Tolerance Factor, t_G	Formation Energy (eV/atom)
$CsGeF_3$	F^-	1.33	1.00	-3.90
	Cs^+	1.90		
	Ge^{2+}	0.96		

Table 3: The elastic stiffness tensor (Cij in GPa) of $CsGeF_3$ Perovskite

Perovskite	XC Functional	C_{11} (GPA)	C_{12} (GPA)	C_{44} (GPA)
$CsGeF_3$	PZ-LDA	163.1835	80.8171	53.1518
	PBE-GGA	111.1645	39.3242	48.9457
	WC-GGA	154.0248	71.5817	51.2297

Elastic properties

The elastic properties of the $CsGeF_3$ perovskite material such as elastic constants via Quantum Espresso code and THERMO_PW using different exchange potentials (PZ_LDA, PBE_GGA, and WC_GGA) is very essential in determining whether or not the studied perovskites are stable elastically and mechanically.

As shown in Fig. 5 (a), these phases are mechanically stable because all of the frames under investigation have elastic constants (Cij) of positive values and meet the mechanical stability requirements. For a cubic crystal system, these criteria require the elastic constants to meet the conditions outlined in the equations below [16]:

$$C_{11} > 0, \quad (5)$$

$$C_{11} + 2C_{12} > 0, \quad (6)$$

$$C_{11} - C_{12} > 0 \quad (7)$$

$$C_{44} > 0 \quad (8)$$

$$C_{12} = C_{13} = C_{21} = C_{23} = C_{31} = C_{32} \quad (9)$$

Mechanical properties

The estimated $CsGeF_3$ perovskite single independent elastic stiffness constants (Cij in GPa) provide a connection between the dynamical and mechanical activity of crystals [17]. These constants are useful indicators in industrial applications and are crucial in investigating the material's strength. The mechanical parameters of the materials under study, such as shear modulus G, Young's modulus E, bulk modulus B, Pugh's ratio r, Poisson's ratio v, machinability index μ_m, Vickers hardness H_v, and anisotropy ratio A, are computed using Voig-Reuss-Hill approximation given by the equations below [16]:

$$B = B_H = \frac{B_V + B_R}{2} \quad (10)$$

$$G = G_H = \frac{G_V + G_R}{2} \quad (11)$$

The average bulk modulus and shear modulus values for each material listed in Table 4 can be computed using equations (10) and (11). The above equations (10 and 11) can be used to calculate Young's modulus (E), Poisson's ratio (v), and Pugh ratio (r) as follows:

$$E = \frac{9BG}{3B+G} \quad (12)$$

$$v = \frac{3B-2G}{2(3B+G)} \quad (13)$$

$$r = \frac{B}{G} \quad (14)$$

The machinability index (μ_m) can be found out using the given relation [18]:

$$\mu_m = \frac{B}{C_{44}} \quad (15)$$

The Vickers hardness (H_V) is formulated using Teter's empirical relation, where G is the shear modulus in GPa and H_V is in GPa (multiply by 9.807 to convert to kg/mm^2) as [19, 20]:

$$H_V = 0.151 \times G \quad (16)$$

A material's isotropy or anisotropy can be ascertained using the elastic stiffness constants, shear moduli, and bulk moduli. The factor of anisotropy A [21] is stated as follows:

$$A = \frac{2C_{44}}{C_{11} - C_{12}} \quad (17)$$

Table 4 shows the elastic parameters of $CsGeF_3$ perovskite in different exchange-correlation functionals (PZ, PBE and WC).

A key elastic parameter that demonstrates how well a material can tolerate deformation (plastic) is the volume stress-to-strain ratio, or B. A high value of B suggests that the height can tolerate volume or plastic distortion [17]. According to Fig. 5(b) and Table 4, CsGeF3 (PZ_LDA) has the greatest bulk modulus (108.27 GPa) of all the compounds' exchange-correlation functionals, suggesting that it can withstand plastic deformation better (very resistant to compression) than other materials. $CsGeF_3$ (PZ) > $CsGeF_3$ (WC) > $CsGeF_3$ (PBE) is the order of bulk modulus for all the materials according to their exchange-correlation functionals.

The shear modulus (G) measures a material's resistance to shear deformation based on the ratio of shear stress to shear strain, is another crucial elastic parameter. The frameworks under study have the following shear modulus sequence: $CsGeF_3$ (PZ) > $CsGeF_3$ (WC) > $CsGeF_3$ (PBE). But compared to the others, $CsGeF_3$ (PZ) has the greatest G value (Moderate resistance), suggesting that it is more resilient to shear deformation.

Young's modulus, E, is another important elastic quantity that establishes a material's capacity to withstand stress longitudinally. After analysing and contrasting each structure as shown in Table 4 and Figure 5(b), it was found that $CsGeF_3$ has a high value of E, indicating that it has the best ability to withstand longitudinal stress compared to other compounds (i.e., good stiffness).

Another important bulk parameter to understand the ductile/brittle nature is the Poisson ratio, ν which measures how much a material expands laterally when longitudinally stretched based on this criterion; $\nu > 0.26 \rightarrow$ ductile material and $\nu < 0.26 \rightarrow$ brittle material or Pugh ratio, *r* which uses the bulk - shear modulus ratio (B/G), where if a substance's $r > 1.75 \rightarrow$ ductile material and $r < 1.75 \rightarrow$ brittle material as per this criterion [22]. As per the following standards, the studied $CsGeF_3$ perovskite with PZ_LDA & WC_GGA are ductile in nature due to strong ionic bonding whereas, with PBE_GGA show brittle nature due to stronger covalent character [17] (Fig. 5(c) and Table 4).

Table 4: The elastic properties of $CsGeF_3$ perovskite and the same kinds of perovskite frameworks

Perovskites	XC Functional	B (GPA)	G (GPA)	E (GPA)	V	R	μ_m	H_v	A
$CsGeF_3$	PZ	108.27	47.99	125.44	0.31	2.26	2.04	7.25	1.29
	PBE	63.27	43.24	105.65	0.22	1.46	1.29	6.53	1.36
	WC	99.06	46.96	121.66	0.30	2.11	1.93	7.09	1.24

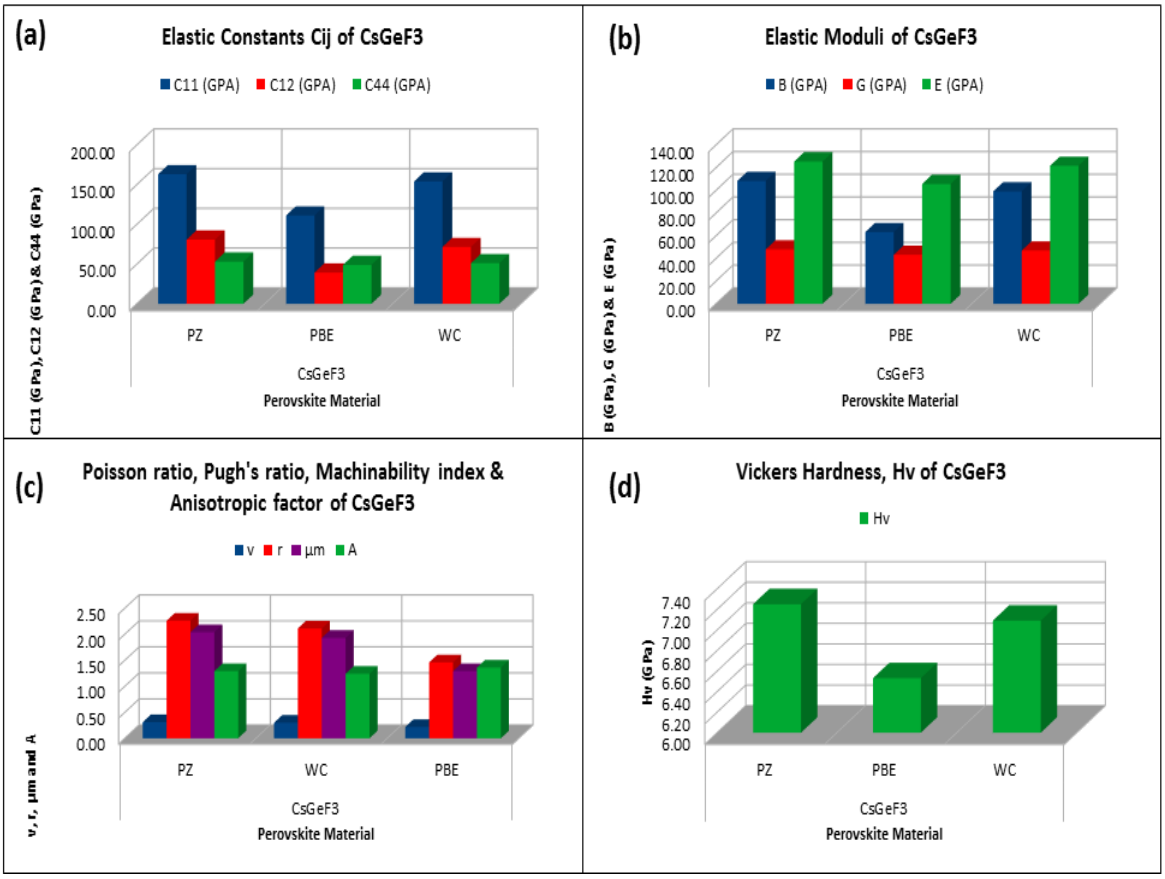

Figure 5: (a) Elastic Constants Cij (GPa); (b) Elastic Moduli B, G & E (GPa); (c) The ratios of Poisson ν, Pugh r, index of machinability μ_m, and Anisotropy, A; (d) Hardness, H_v of $CsGeF_3$ perovskite

The hardness of any material is a different macroscopic bulk property used frequently in the technological and manufacturing industries. In general, plastic deformation regulates the hardness of a substance; therefore, a high-hardness material is better able to resist plastic deformity, whereas a low-hardness material is less able to resist plastic deformity [17, 23]. Consequently, a low-hardness material is utilized for plastic deformation in order to improve the material's machinability. The material is more machinable and damage-tolerant when the hardness value is between 2 and 8 GPa [24]. The $CsGeF_3$ material with PZ-LDA had the highest hardness value in the comparison, demonstrating its greatest capacity to withstand plastic deformation.

These days, a material's ability to be machined is an essential characteristic used in industry to reach targeted productivity at the lowest feasible cost. The machinability index is influenced by a variety of parameters, such as the mechanical equipment's stiffness, cutting form, cutting process, capacity, and hardness [25]. In contrast to PBE from (Fig. 5(c)), it has been noted that the phase $CsGeF_3$ with PZ and WC has a considerable index of machinability among the named compounds, making it very mechanically competent. This study demonstrated the exceptional mechanical capabilities of materials with low bulk, shear, and young's moduli and their potential industrial applications.

The Zener anisotropy factor (A), describes the bulk characteristics that depend on a crystal structure's orientation. Anisotropic materials contain crystals that exhibit peculiar qualities in a specific direction, whereas isotropic materials have crystals with the same properties in all directions. If A = 1, it indicates that the crystal is isotropic; otherwise, it is anisotropic. According to our computations, the $CsGeF_3$ material with all exchange-correlation functionals is anisotropic, but the $CsGeF_3$ with PBE_GGA is more so than the others.

Conclusion

The structural, elastic, and mechanical properties of lead-free $CsGeF_3$ perovskite are investigated in depth using density functional theory (DFT) in this work. The calculated lattice constant was found to be 4.29 Å, 4.33 Å and 4.34 Å for PZ, PBE and WC respectively, which is in close agreement with available data. The calculated elastic constants, C_{11} (163.18 GPa, 111.17 GPa and 154.03 GPa), C_{12} (80.82 GPa, 39.32 GPa and 71.58 GPa) and C_{44} (53.15 GPa, 48.95 GPa and 51.23 GPa) for PZ, PBE and WC respectively. The material is mechanically stable, as evidenced by the estimated elastic constants. The material showed a bulk modulus measurement of ~108 GPa (PZ), which demonstrated its ability to withstand compression pressure. The research investigates the physical characteristics of $CsGeF_3$ while assessing its viability as a solar energy harvesting material that does not use lead-based perovskites. The process creates solar cells that achieve both sustainability and high energy efficiency.

Conflict of interest: The authors declare no conflicts of interest.

References

[1] Glazer, A. M. (1972). The classification of tilted octahedra in perovskites. *Acta Crystallographica Section B: Structural Crystallography and Crystal Chemistry*, 28(11), 3384–3392. https://journals.iucr.org/b/issues/1972/11/00/a09401/a09401.pdf

[2] Goldschmidt, V. M. (1926). Die Gesetze der Krystallochemie. *Die Naturwissenschaften*, 14(21), 477–485. https://doi.org/10.1007/BF01507527

[3] Kojima, A., Teshima, K., Shirai, Y. & Miyasaka, T. (2009). Organometal halide perovskites as visible-light sensitizers for photovoltaic cells. *J. of the American Chemical Society*, 131(17), 6050–6051. https://doi.org/10.1021/ja809598r

[4] Park, N.-G. (2015). Perovskite solar cells: An emerging photovoltaic technology. *Materials Today*, 18(2), 65–72. https://www.sciencedirect.com/science/article/pii/S1369702114002570

[5] Snaith, H. J. (2013). Perovskites: The emergence of a new era for low-cost, high-efficiency solar cells. *The J. of Physical Chem. Letters*, 4(21), 3623–3630. https://doi.org/10.1021/jz4020162

[6] Aslam, M., Mahmood, T. & Naeem, A. (2021). *Organic Inorganic Perovskites: A Low-Cost-Efficient Photovoltaic Material* (Vol. 11). IntechOpen. https://books.google.com/books?hl=en&lr=&id=2KMtEAAAQBAJ&oi=fnd&pg=PA71&dq=Madeeha+Aslam,+Tahira+Mahmood+and+Abdul+Naeem,+Organic+Inorganic+Perovskites:+A+Low-Cost-Efficient+Photovoltaic+Material+(2021).+DOI:+http://dx.doi.org/10.5772/intechopen.94104&ots=wc6h4NGsJu&sig=PABqjHQR8iDqICwbz2uLhVYfmx0

[7] Al-Muhimeed, T. I., Aljameel, A. I., Mera, A., Saad, S., Nazir, G., Albalawi, H., Bouzgarrou, S., Hegazy, H. H. & Mahmood, Q. (2022). First principle study of optoelectronic and mechanical properties of lead-free double perovskites Cs_2 SeX_6 (X = Cl, Br, I). *Journal of Taibah University for Sci.*, 16(1), 155–162. https://doi.org/10.1080/16583655.2022.2035927

[8] Correa-Baena, J.-P., Saliba, M., Buonassisi, T., Grätzel, M., Abate, A., Tress, W. & Hagfeldt, A. (2017). Promises and challenges of perovskite solar cells. *Sci.*, 358(6364), 739–744. https://doi.org/10.1126/science.aam6323

[9] Gilani, S. S., Tariq, S., Jamil, M. I., Tahir, B., & Faridi, M. A. (2018). Elucidating DFT study on structural, electronic, thermal and elastic properties of $SrTcO_3$ by using GGA and mBJ approach. *Chinese Journal of Physics*, 56(1), 308–314. https://www.sciencedirect.com/science/article/pii/S0577907317315721

[10] Ke, W., Stoumpos, C. C. & Kanatzidis, M. G. (2019). "Unleaded" perovskites: Status quo and future prospects of tin-based perovskite solar cells. *Advanced Materials*, 31(47), 1803230. https://doi.org/10.1002/adma.201803230

[11] Magdalin, A. E., Nixon, P. D., Jayaseelan, E., Sivakumar, M., Devi, S. K. N., Subathra, M. S. P., Kumar, N. M. & Ananthi, N. (2023). Development of lead-free perovskite solar cells: Opportunities, challenges, and future technologies. *Results in Engineering*, 101438. https://www.sciencedirect.com/science/article/pii/S2590123023005650

[12] Abd Mutalib, M., Ahmad Ludin, N., Nik Ruzalman, N. A. A., Barrioz, V., Sepeai, S., Mat Teridi, M. A., Su'ait, M. S., Ibrahim, M. A. & Sopian, K. (2018). Progress towards highly stable and lead-free perovskite solar cells. *Materials for Renewable and Sustainable Energy*, 7(2), 7. https://doi.org/10.1007/s40243-018-0113-0

[13] Selmani, Y., Labrim, H., Mouatassime, M. & Bahmad, L. (2022). Structural, optoelectronic and thermoelectric properties of Cs-based fluoroperovskites $CsMF_3$ (M= Ge, Sn or Pb). *Materials Science in Semiconductor Processing*, 152, 107053. https://www.sciencedirect.com/science/article/pii/S1369800122005820

[14] Houari, M., Bouadjemi, B., Haid, S., Matougui, M., Lantri, T., Aziz, Z., Bentata, S. & Bouhafs, B. (2020). Semiconductor behavior of halide perovskites $AGeX_3$ (A = K, Rb and Cs; X = F, Cl and Br): First-principles calculations. *Indian J. of Physics*, 94(4), 455–467. https://doi.org/10.1007/s12648-019-01480-0

[15] Monkhorst, H. J. & Pack, J. D. (1976). Special points for Brillouin-zone integrations. *Physical Review B*, 13(12), 5188–5192. https://doi.org/10.1103/PhysRevB.13.5188

[16] Ahmad, I. (2014). Elastic constants of cubic crystals. *Computational Materials Science*. https://doi.org/10.1016/J.COMMATSCI.2014.08.027

[17] Rahman, Md. A., Mostari, F., Hasan, Md. Z., Irfan, A., Rahman, Md. F., Hosain, M. J., Mouna, S. C., Chowdhury, I. A., Rasheduzzaman, Md. & Choudhury, M. S. H. (2023). First principles study on the structural, elastic, electronic, optical and thermal properties of lead-free perovskites $CsCaX_3$(X=F, Cl, Br). *Physica B: Condensed Matter*, 669, 415260. https://doi.org/10.1016/j.physb.2023.415260

[18] Sun, Z., Music, D., Ahuja, R. & Schneider, J. M. (2005). Theoretical investigation of the bonding and elastic properties of nanolayered ternary nitrides. *Physical Review B*, 71(19), 193402. https://doi.org/10.1103/PhysRevB.71.193402

[19] Chen, X.-Q., Niu, H., Li, D. & Li, Y. (2011). Modeling hardness of polycrystalline materials and bulk metallic glasses. *Intermetallics*, 19(9), 1275–1281. https://doi.org/10.1016/j.intermet.2011.03.026

[20] Jubair, M., Tanveer Karim, A. M. M., Nuruzzaman, M., Roknuzzaman, M. & Zilani, M. A. K. (2021). Pressure dependent structural, elastic and mechanical properties with ground state electronic and optical properties of half-metallic Heusler compounds Cr2YAl (Y=Mn, Co): First-principles study. *Heliyon*, 7(12), e08585. https://doi.org/10.1016/j.heliyon.2021.e08585

[21] Parvin, F. & Naqib, S. H. (2019). Structural, elastic, electronic, thermodynamic, and optical properties of layered $BaPd_2As_2$ pnictide superconductor: A first principles investigation. *Journal of Alloys and Compounds*, 780, 452–460. https://doi.org/10.1016/j.jallcom.2018.12.021

[22] Pugh, S. F. (1954). XCII. Relations between the elastic moduli and the plastic properties of polycrystalline pure metals. *The London, Edinburgh, and Dublin Philosophical Magazine and Journal of Science*. (world). https://doi.org/10.1080/14786440808520496

[23] Atarah, S. A. (2023). A first-principles study of the Mechanical Stability and Electronic Properties of Lead-free Halide Inorganic Double Perovskites Cs_2InAgX_6 (X= F, Br, Cl, I). *Science and Development*, 7(2), 17–31. https://www.ajol.info/index.php/jsdugs/article/view/259061

[24] Barsoum, M. W. & Radovic, M. (2011). Elastic and Mechanical Properties of the MAX Phases. *Annual Review of Materials Research*, 41, 195–227. https://doi.org/10.1146/annurev-matsci-062910-100448

[25] Naher, M. I. & Naqib, S. H. (2021). An ab-initio study on structural, elastic, electronic, bonding, thermal, and optical properties of topological Weyl semimetal TaX (X = P, As). *Scientific Reports*, 11(1), 5592. https://doi.org/10.1038/s41598-021-85074-z

Citing this Article

Otto, M. S., Liman, M. S., Lawal, A., Abdullahi, A. D., & Usman, F. M. (2026). First-principles computation of cubic $CsGeF_3$ perovskite's structural, elastic, and mechanical properties. *Lafia Journal of Scientific and Industrial Research*, *4*(1), 198–205. https://doi.org/10.62050/ljsir2026.v4n1.806